BIOCHEMISTRY
including biophysical chemistry & molecular biology
Article

Biochemistry **2009,** *48,* 4455–4465 4455
DOI:10.1021/bi900179j

Spectral and Kinetic Characterization of Intermediates in the Aromatization Reaction Catalyzed by NikD, an Unusual Amino Acid Oxidase[†]

Robert C. Bruckner and Marilyn Schuman Jorns*

Department of Biochemistry and Molecular Biology, Drexel University College of Medicine, Philadelphia, Pennsylvania 19102

Received February 4, 2009; Revised Manuscript Received April 7, 2009

ABSTRACT: The flavoenzyme nikD, a 2-electron acceptor, catalyzes a remarkable aromatization of piperideine-2-carboxylate (P2C) to picolinate, an essential component of nikkomycin antibiotics. Steady-state kinetic data are indicative of a sequential mechanism where oxygen reacts with a reduced enzyme·dihydropicolinate (DHP) complex. The kinetics observed for complex formation with competitive inhibitors are consistent with a one-step binding mechanism. The anaerobic reaction with P2C involves three steps. The first step yields an enzyme·substrate charge transfer complex likely to contain the electron-rich P2C enamine. Calculated rates of formation and dissociation of the nikD·P2C complex are similar to those observed for the enzyme·1-cyclohexenoate complex. Formation of a reduced enzyme·DHP complex, $(EH_2 \cdot DHP)^{ini}$, occurs in a second step that exhibits a hyperbolic dependence on substrate concentration. The limiting rate of nikD reduction is at least 10-fold faster than the turnover rate observed with unlabeled or [4,4,5,5,6,6-D_6]-P2C and exhibits a kinetic isotope effect (KIE = 6.4). The observed KIE on $K_{d\ apparent}$ (4.7) indicates that P2C is a sticky substrate. Formation of a final reduced species, $(EH_2 \cdot DHP)^{fin}$, occurs in a third step that is independent of P2C concentration and equal to the observed turnover rate. The observed KIE (3.3) indicates that the final step involves cleavage of at least one C−H bond. Tautomerization, followed by isomerization, of the initial DHP intermediate can produce an isomer that could be oxidized to picolinate in a reaction that satisfies known steric constraints of flavoenzyme reactions without the need to reposition a covalently tethered flavin or tightly bound intermediate.

NikD is a flavoprotein oxidase that plays an essential role in the biosynthesis of nikkomycins. Nikkomycins comprise a group of related peptidyl nucleoside antibiotics that resemble the natural substrate of chitin synthase. Chitin, the second most abundant polysaccharide in nature, is an integral component of the cell wall in fungi and the exoskeleton of invertebrates but is not found in mammals. Nikkomycins are potent antifungal agents that act by competitively inhibiting chitin synthase. Nikkomycins are therapeutically effective in treating human fungal infections that are especially prevalent in immunocompromised patients and are also useful in agriculture as easily degraded insecticides that are nontoxic for mammals (*1*).

The nikkomycin peptide is synthesized by a nonribosomal pathway and contains an N-terminal pyridyl moiety, derived from L-lysine, that is essential for antibiotic function. Synthesis of the pyridyl moiety is initiated by an α-aminotransferase that converts L-lysine to piperideine-2-carboxylate (P2C[1]) (*2*), a compound that can exist in imine and enamine tautomeric forms (*3*−*5*). Picolinate is produced in a remarkable aromatization reaction catalyzed by nikD, involving an overall 4-electron oxidation of P2C (Scheme 1) (*6*). NikD contains covalently bound FAD (8α-S-cysteinyl-FAD) (*7*), acts as an obligate 2-electron acceptor (*6*), and is a member of a family of monomeric amino acid oxidases (M_r ~44 kDa) that all contain a single covalently bound flavin (*8*−*13*). A nikD-like reaction is implicated in the biosynthesis of the pyridyl moiety found in streptogramin antibiotics that are used to treat multidrug-resistant Gram-positive bacterial infections (*14*).

There are six possible paths for the initial 2-electron oxidation of P2C to dihydropicolinate (DHP), depending in part on whether nikD oxidizes the imine or enamine tautomer. Oxidation of the bond between N(1) and C(6) in the enamine tautomer, as indicated in Scheme 1, is the most likely path, as judged by results obtained in structural and biochemical studies (*7*, *15*). The second 2-electron oxidation step is more problematic because it would seem to involve oxidation of a bond at a different location within the DHP intermediate, a scenario that requires an apparent change in regiospecificity. This feature would distinguish the nikD reaction from the overall 4-electron oxidation reactions catalyzed by the flavoenzymes choline oxidase, thiamine oxidase, and glycolate oxidase because the two successive 2-electron

[†]This work was supported in part by Grant AI 55590 (M.S.J.) from the National Institutes of Health.

*To whom correspondence should be addressed. Phone: (215) 762-7495. Fax: (215) 762-4452. E-mail: marilyn.jorns@drexelmed.edu.

[1]Abbreviations: FAD, flavin adenine dinucleotide, P2C, piperideine-2-carboxylate; CHA, 1-cyclohexenoate; D_6-P2C, [4,4,5,5,6,6-D_6]-P2C; MeSeA, methylselenoacetate, KIE, kinetic isotope effect; ES complex, enzyme·substrate complex.

Published on Web 4/8/2009

Scheme 1: nikD-Catalyzed Oxidation of P2C to Picolinate[a]

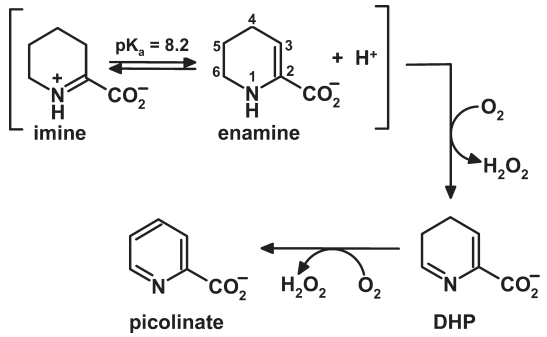

[a] The dihydropicolinate (DHP) intermediate shown is one of six possible isomers.

oxidation steps, required to convert alcohol substrates to carboxylic acids, occur at the same carbon (*16*−*18*). Similarly, the three successive 2-electron oxidation steps in estrogen biosynthesis occur at the same exocyclic carbon in the impressive aromatization reaction catalyzed by aromatase cytochrome P450 (*19*).

NikD exhibits two absorption maxima in the visible region, as expected for a flavoprotein, plus an unusual long-wavelength absorption band due to charge-transfer interaction of the flavin with Trp355 (*20*). Crystal structures determined for open and closed forms of the nikD·picolinate complex reveal two distinct ligand binding modes and two different orientations of the side chain of Trp355 (*15*). In the open form, the rings of picolinate and FAD are nearly perpendicular, a binding mode incompatible with redox catalysis. However, the rings of Trp355 and FAD are parallel in the open form, an orientation that promotes charge-transfer interaction. In the closed form, the rings of FAD and picolinate are parallel, a binding mode compatible with redox catalysis. The rings of Trp355 and FAD are perpendicular in the closed form, an orientation that is incompatible with charge-transfer interaction. The observed structures led us to propose a two-step mechanism for substrate binding: (i) P2C binds to an open form with Trp355 stacked atop the flavin to produce an unstable redox-inactive open complex, otherwise similar to the corresponding crystalline complex with picolinate; (ii) the open nikD·P2C complex undergoes a conformational change to yield a more stable redox-active closed complex, similar to the crystalline closed nikD·picolinate complex (*20*).

In this article, we investigate the mechanism of ligand binding and the initial 2-electron oxidation of P2C. Results obtained with analogues for the imine and enamine forms of P2C do not support a 2-step binding model but are consistent with a one-step approach to equilibrium in a reaction that is orders of magnitude slower than expected for a diffusion-controlled process. Steady-state and presteady-state kinetic studies with unlabeled and deuterium-labeled substrate have enabled spectral and kinetic characterization of two intermediates in the conversion of P2C to DHP. Unexpectedly, these studies also provide important insight into the conundrum of the second 2-electron step that produces picolinate.

EXPERIMENTAL PROCEDURES

Materials. [3,3,4,4,5,5,6,6-D$_8$]-L-lysine was purchased from CDN Isotopes Inc. Benzyl chloroformate and picolinate were purchased from Sigma. Methylselenoacetate was a generous gift from Dr. Louis Silks (National Stable Isotope Resource at Los Alamos). 1-Cyclohexenoate was obtained from Aldrich. ε-*N*-Carbobenzoxy-L-lysine was purchased from Fluka. L-Amino acid oxidase was isolated from *Crotalus adamanteus* venom (Biotoxins, Inc.), as previously described (*21*, *22*). Unlabeled P2C was prepared as described by Bruckner et al. (*6*).

Enzyme Isolation and Steady-State Kinetic Studies. Recombinant wild-type nikD was isolated from cells [*Escherichia coli* Bl21(DE3)/pDV101] grown in Terrific Broth, as previously described (*7*). Steady-state kinetic studies with nikD at various concentrations of P2C and oxygen were conducted in 100 mM potassium phosphate buffer at pH 8.0, at 25 °C using screw-cap cuvettes (Spectrocell) that were equipped with a Teflon-silicon membrane and equilibrated at 25 °C with water-saturated gas mixtures containing 10, 21, 44, or 100% oxygen (balance nitrogen), as previously described (*23*). Reactions were monitored by measuring picolinate formation at 264 nm (ε = 3980 M^{-1} cm^{-1}) (*6*). Steady-state kinetic parameters were estimated by fitting an equation for a sequential mechanism (eq 1, A = P2C and B = oxygen) to the data.

$$V = \frac{V_{max}[A][B]}{K_{ia}K_b + K_a[B] + K_b[A] + [A][B]} \quad (1)$$

Synthesis of Deuterium-Labeled P2C. [3,3,4,4,5,5,6,6-D$_8$]-L-lysine was converted to a copper complex of ε-*N*-carbobenzoxy-L-lysine by following the method of Neuberger and Sanger (*24*). Free [3,3,4,4,5,5,6,6-D$_8$]-ε-*N*-carbobenzoxy-L-lysine was prepared by treatment of the copper complex with sodium sulfide (*25*) and then converted to deuterium-labeled P2C by following a method previously used to prepare unlabeled P2C (*6*). Briefly, [3,3,4,4,5,5,6,6-D$_8$]-ε-*N*-carbobenzoxy-L-lysine was oxidized to [3,3,4,4,5,5,6,6-D$_8$]-ε-*N*-carbobenzoxy-α-keto-ε-amino-caproic acid using L-amino acid oxidase. The carbobenzoxy group was removed by treatment with acetic acid-HBr, forming [3,3,4,4,5,5,6,6-D$_8$]-α-keto-ε-amino-caproic acid as a transient intermediate that spontaneously cyclizes to yield the hydrobromide salt of the imine tautomer of P2C (D$_8$-P2C).

Steady-State Spectroscopy. Absorption spectra were recorded using an Agilent Technologies 8453 diode array spectrometer. All spectra are corrected for dilution. Enzyme concentration was determined at pH 8.0 based on its absorbance at 456 nm (ε = 11,200 M^{-1} cm^{-1}) (*7*). The dissociation constant of the nikD·methylselenoacetate complex was determined by fitting a standard binding curve ($\Delta A_{obs} = \Delta A_{max}$[ligand]/($K_d$ + [ligand]) to the data. The spectrum corresponding to 100% complex formation was calculated as previously described (*26*). Spectrophotometric titration data with picolinate or 1-cyclohexenoate were analyzed by using an equation for a tight binding inhibitor (eq 2; X_T and E_T are total ligand and enzyme concentrations, respectively). Fitting of binding equations was conducted by using Sigma Plot 10 (Systat Software).

$$\Delta A_{obs} = \frac{\Delta A_{max}}{2E_T}\left[(X_T + E_T + K_d) - \sqrt{(X_T + E_T + K_d)^2 - (4E_T X_T)}\right] \quad (2)$$

Rapid Reaction Spectroscopy. Rapid reaction kinetic measurements were performed by using a Hi-Tech Scientific SF-61DX2 stopped-flow spectrometer. Data were collected in log mode to maximize the number of points acquired during the early phase of each reaction. All spectra or single-wavelength kinetic

traces are the averages of at least three replicate shots. The kinetics of binding of picolinate, 1-cyclohexenoate, or methylselenoacetate were monitored by using photomultiplier detection, unless otherwise indicated, in aerobic 100 mM potassium phosphate buffer at pH 8.0, at 25 °C. Reductive half-reactions with unlabeled or deuterium-labeled P2C were monitored by using diode array detection in anaerobic 100 mM potassium phosphate buffer at pH 8.0, containing 50 mM glucose and glucose oxidase (14.7 units/mL). All components, except glucose oxidase, were placed in the main compartment of a tonometer. Glucose oxidase was tipped from a side arm into the main compartment after the solutions were made anaerobic by multiple cycles of evacuation, followed by flushing with oxygen-scrubbed argon. The entire flow circuit of the stopped-flow spectrometer was made anaerobic by an overnight incubation with anaerobic buffer containing 50 mM glucose and glucose oxidase (14.7 units/mL). All spectra are corrected for a small spectral contribution from P2C in the near-ultraviolet region. Fitting of single-wavelength kinetic traces was conducted by using Sigma Plot 10 (Systat Software), KinetAsyst 3 (TgK Scientifc), or Kinetic Studio (TgK Scientific). Global analyses of absorption spectra acquired during reductive half-reactions were performed using Specfit 3.0, a software package that generates calculated spectra of intermediates and rate constants for intermediate formation and decay.

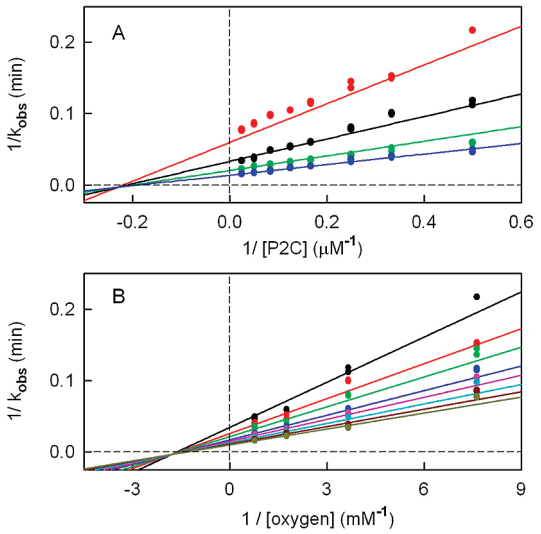

FIGURE 1: Steady-state kinetic analysis of P2C oxidation by nikD. Reactions were conducted in 100 mM potassium phosphate buffer at pH 8.0, at 25 °C. Panel A: Data obtained at 0.13, 0.27, 0.57, and 1.29 mM oxygen are shown by the red, black, green, and blue circles, respectively. Panel B: Data obtained at 2.0, 3.0, 4.0, 6.0, 8.0, 12.0, 20.0, and 40 μM P2C are shown by the black, red, green, blue, magenta, cyan, brown, and dark yellow circles, respectively. The solid lines in panels A and B were obtained by fitting eq 1 to the data.

RESULTS

Steady-State Turnover of NikD with P2C. Turnover rates at various concentrations of unlabeled P2C and oxygen were measured by monitoring picolinate formation at 264 nm (*6*). Double reciprocal plots of reaction rate versus P2C at different oxygen concentrations or versus oxygen at different P2C concentrations are linear and intersect to the left of the *y*-axis, just below the *x*-axis (Figure 1). The results are consistent with a sequential mechanism where oxygen reacts with a reduced enzyme·DHP complex to yield an oxidized enzyme·DHP complex that can undergo a second redox cycle to produce picolinate. The minimal mechanism shown in Scheme 2 assumes that dissociation of the oxidized enzyme·DHP complex is negligible, consistent with other observations, as will be discussed. The steady-state kinetics parameters listed in Table 1 were obtained by fitting an equation for a sequential mechanism to the data.

Kinetics of Picolinate and 1-Cyclohexenoate Binding to NikD. Crystal structures observed for open and closed forms of the nikD·picolinate complex suggested that formation of the enzyme·P2C complex might occur via a two-step mechanism (*15*, *20*). We reasoned that the kinetics of ligand binding to nikD might be more easily characterized in studies with competitive inhibitors, such as picolinate, the product of the catalytic reaction, or 1-cyclohexenoate (CHA), a 1-deaza analogue of the enamine form of P2C. Fortunately, the binding of these inhibitors is fairly slow and can be readily monitored in a stopped-flow spectrometer at 25 °C.

The spectral course observed for the time-dependent formation of the nikD·picolinate complex in the presence of excess ligand (Figure 2A) is identical to that observed in steady-state titration studies (*7*). Picolinate binding results in a substantial increase in the intensity of the absorption peak at 456 nm, accompanied by the loss of a long-wavelength absorption band attributable to charge-transfer interaction between FAD and Trp355 (*20*). Apparent first-order rate constants obtained

Scheme 2: Minimal Steady-State Kinetic Mechanism for the nikD-Catalyzed Conversion of P2C to Picolinate (P) without Release of the DHP Intermediate[a]

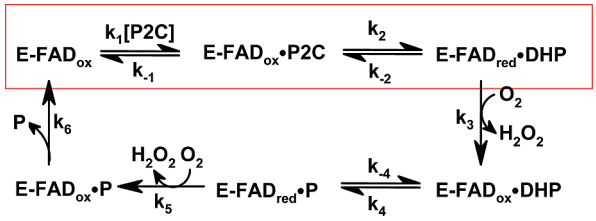

[a] The red box indicates the portion of the overall reaction that is monitored in reductive half-reaction studies.

for the formation of the picolinate complex are independent of the observation wavelength (Figure 2B). The observed rate constants exhibit a linear dependence on inhibitor concentration (Figure 3A). In contrast, a hyperbolic dependence on ligand concentration with a finite *y*-intercept is expected for a two-step binding mechanism (*26*). The results are, however, consistent with a simple one-step approach to equilibrium where $k_{obs} = k_f$[ligand] + k_r. Rate constants for complex formation (k_f) and dissociation (k_r) were obtained from the slope and intercept, respectively, of this plot. The kinetically determined dissociation constant ($K_d = k_r/k_f = 280 \pm 30$ μM) is in excellent agreement with a value determined by steady-state titration ($K_d = 290 \pm 40$ μM) (Table 2). The rate constant determined for dissociation of the nikD·picolinate complex ($k_r = 8.0 \pm 0.7$ s^{-1}) corresponds to the rate constant for the last step in the minimal steady-state kinetic mechanism (k_6) (see Scheme 2). The results indicate that this step is only 3-fold faster than turnover ($k_{cat} = 2.3 \pm 0.2$ s^{-1}), suggesting that product release may be partially rate-determining.

The spectral properties of the nikD·CHA complex are very similar to those observed for the picolinate complex (*7*), but the

Table 1: Kinetic Parameters for the Reaction of Wild-Type nikD with P2C at pH 8.0. 25 °C

	reductive half-reaction[a]				steady-state turnover				
	k_{lim} (s^{-1})	k_{slow} (s^{-1})	$K_{d\ app}$ (μM)	$k_{lim}/K_{d\ app}$ ($M^{-1}\ s^{-1}$)	k_{cat} (s^{-1})	$k_{cat}/K_{m\ P2C}$ ($M^{-1}\ s^{-1}$)	$k_{cat}/K_{m\ O2}$ ($M^{-1}\ s^{-1}$)	$K_{m\ P2C}$ (μM)	$K_{i\ P2C}$ (μM)
H−P2C					2.3 ± 0.2	$2.0 \pm 0.3 \times 10^5$	$2.6 \pm 0.2 \times 10^3$	21 ± 2	2.9 ± 0.8
biphasic	53 ± 1	2.7 ± 0.1	260 ± 20	$2.0 \pm 0.2 \times 10^5$					
D_6-P2C					0.89 ± 0.04	$0.74 \pm 0.07 \times 10^5$	$1.9 \pm 0.2 \times 10^3$	12 ± 1	3 ± 1
triphasic	8.25 ± 0.01	0.822 ± 0.008	55.2 ± 0.7	$1.49 \pm 0.02 \times 10^5$					
biphasic	8.02 ± 0.07	0.75 ± 0.03	51 ± 3	$1.6 \pm 0.1 \times 10^5$					
global	7.86 ± 0.03	0.81 ± 0.01	49 ± 1	$1.60 \pm 0.03 \times 10^5$					

[a] The reaction occurs in three phases, as judged by absorbance changes at 456 nm: (1) an initial lag (H−P2C) or an initial increase in absorbance (D_6-P2C); (2) a rapid decrease in absorbance (k_{fast}) that exhibits a hyperbolic dependence on the concentration of P2C ($k_{obs} = k_{lim}[P2C]/(K_{d\ app} + [P2C])$; and (3) a slow decrease in absorbance (k_{slow}) that is independent of the concentration of P2C. Values for k_{fast} and k_{slow}, with H-P2C were obtained by fitting a double-exponential equation ($y = Ae^{-k_{fast}t} + Be^{-k_{slow}t} + C$) to the observed decrease in absorbance at 456 nm (phases 2 and 3). Values for k_{fast} and k_{slow} with D_6-P2C were obtained by fitting a triple-exponential equation ($y = Ae^{-k_{initial}t} + Be^{-k_{fast}t} + Ce^{-k_{slow}t} + D$) to the total absorbance change at 456 nm (phases 1, 2, and 3). Similar results were obtained by fitting a double-exponential equation to the decrease in absorbance at 456 nm observed with D_6-P2C (phases 2 and 3) or by global analysis of the entire spectral course observed with D_6-P2C, as described in Results.

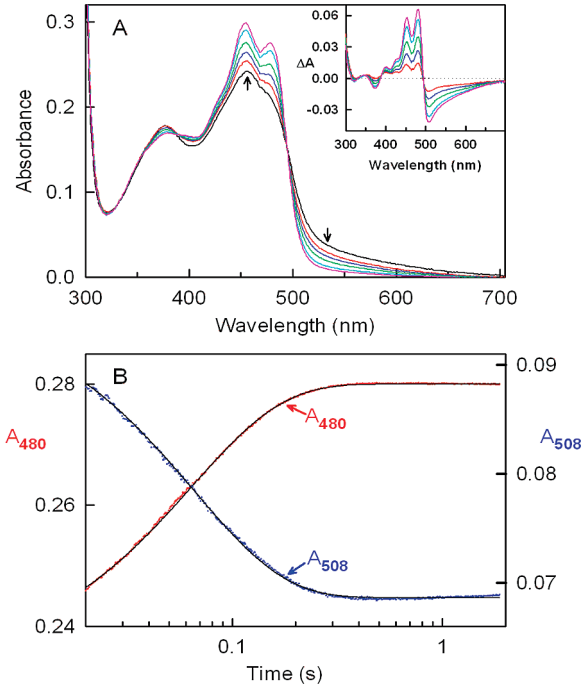

FIGURE 2: Kinetics of formation of the nikD·picolinate complex. Reactions were conducted in 100 mM potassium phosphate buffer at pH 8.0, at 25 °C. Panel A shows the spectral course of complex formation as monitored using a stopped-flow diode array spectrometer. Arrows indicate the directions of the observed spectral changes. The black curve is the spectrum of free nikD. The red, blue, green, cyan, and magenta curves were recorded at 2.24 ms, 5.24 ms. 9.74 ms, 20.2 ms, and 1.425 s, respectively, after mixing nikD with 3000 μM picolinate. The inset shows the corresponding difference spectra, calculated by subtracting the spectrum observed for free nikD. Panel B shows the kinetics of complex formation with 300 μM picolinate. Reactions were monitored at 480 nm (red circles) or 508 nm (blue circles) using a stopped-flow spectrometer in photomultiplier mode. The black lines were obtained by fitting a single-exponential equation ($y = Ae^{-kt} + B$) to the data.

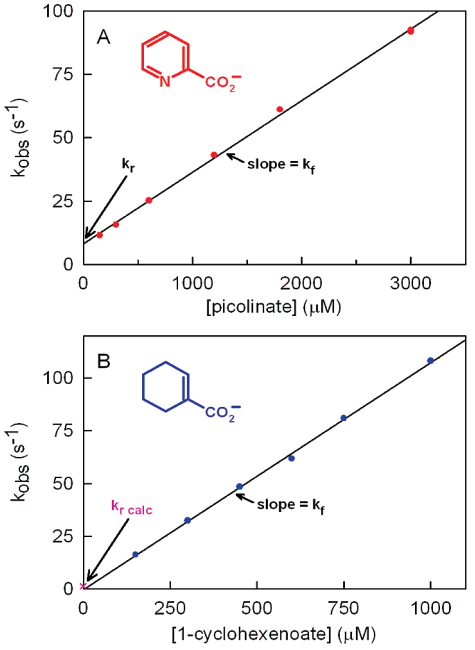

FIGURE 3: Effect of ligand concentration on the observed rate of complex formation with picolinate (panel A) or 1-cyclohexenoate (panel B). Reactions were conducted in 100 mM potassium phosphate buffer at pH 8.0 at 25 °C. Complex formation was monitored at 480 nm using a stopped-flow spectrometer in photomultiplier mode. The solid lines in each panel were obtained by linear regression analysis of the data (red or blue circles). The value for $k_{r\ calc}$ indicated in panel B was determined as described in Table 2.

complex formed with CHA is ~20-fold more stable. Apparent first-order rate constants obtained for the formation of the nikD·CHA complex exhibit a linear dependence on CHA concentration (Figure 3B), consistent with a one-step binding mechanism. Formation of the nikD·CHA complex is ~4-fold faster, whereas dissociation of the complex is ~6-fold slower, as compared with the picolinate complex (Table 2).

Spectral, Thermodynamic, and Kinetic Characterization of a NikD Complex Formed with Methylselenoacetate. The nikD complexes formed with picolinate, CHA, or various other inhibitors (e.g., benzoate, pyrrole-2-carboxylate, and 2-furoate) (*7*) do not exhibit significant long-wavelength absorption and hence provide no evidence for charge-transfer interaction between the ligands and FAD, as expected for these electron-poor substrate analogues. P2C can, however, exist as an electron-poor protonated imine or an electron-rich enamine (see Scheme 1). Methylselenoacetate ($CH_3SeCH_2CO_2^-$) (MeSeA) can be viewed as an electron-rich analogue of the reactive center in the enamine form of P2C. Importantly, MeSeA does form a spectrally detectable complex with nikD ($K_d = 1.07 \pm 0.04$ mM), characterized by an increase in absorbance in both the 456 nm and

Table 2: Kinetics of Formation of nikD Complexes with Product, Substrate, and Substrate Analogues[a]

	k_f (M^{-1} s^{-1})	k_r (s^{-1})	K_d (kinetic)[b] (μM)	K_d (static) (μM)
picolinate	$2.83 \pm 0.04 \times 10^4$	8.0 ± 0.7	280 ± 30	290 ± 40 (300)[c]
P2C[d]	$2.2 \pm 0.2 \times 10^5$	3.8 ± 0.3	17 ± 2	
1-cyclohexenoate	$1.08 \pm 0.02 \times 10^5$	1.4 ± 0.1[e]		12.8 ± 0.9 (16)[c]
methylselenoacetate	$2.3 \pm 0.1 \times 10^3$	5.4 ± 0.4	$2.4 \pm 0.2 \times 10^3$	$1.07 \pm 0.04 \times 10^3$

[a] Measurements were made in 100 mM potassium phosphate at pH 8.0, at 25 °C. [b] K_d (kinetic) = k_r/k_f. [c] Values previously reported by Venci et al. (*7*). [d] Values for k_f and k_r were calculated using the values obtained for $K_{d\ app}$ and k_{cat} in reductive half-reaction studies with unlabeled and deuterium-labeled P2C (see Table 1), as discussed in the text. [e] Calculated using the value obtained for k_r and the K_d determined by steady-state titration.

long-wavelength regions (Figure 4A). The nikD·MeSeA complex exhibits a charge-transfer band at 581 nm, as estimated by the position of the peak observed in the difference spectrum (Figure 4A, inset). The results suggest that a nikD complex with the enamine tautomer of P2C would also exhibit evidence of charge-transfer interaction. Apparent first-order rate constants obtained for the formation of the nikD·MeSeA complex exhibit a linear dependence on ligand concentration (Figure 4B), as observed with picolinate and CHA. The charge-transfer complex formed with MeSeA is about 100-fold less stable as compared with the nikD·CHA complex, a difference that is mainly due to a decrease in the rate of complex formation (Table 2).

Kinetics of the Reductive Half-Reaction of NikD with Unlabeled P2C. The kinetics of the initial 2-electron oxidation of P2C to DHP were investigated by monitoring the anaerobic reaction of nikD with various concentrations of P2C in a stopped-flow spectrometer. The reaction with 100 μM P2C exhibits an initial lag, followed by a decrease in absorption at 456 nm, as expected for flavin reduction. The lag becomes progressively smaller at higher substrate concentrations and is not detectable at 2500 μM P2C (Figure 5A). The observed decrease in absorbance at 456 nm exhibits biphasic kinetics ($y = Ae^{-k_{fast}t} + Be^{-k_{slow}t} + C$) at all tested P2C concentrations (100 to 2500 μM). The rate observed for the initial rapid phase (k_{fast}) exhibits a hyperbolic dependence on the concentration of P2C ($k_{obs} = k_{lim}[P2C]/(K_{d\ app} + [P2C])$ (Figure 5B). The limiting rate at saturating P2C ($k_{lim} = 53 \pm 1\ s^{-1}$) is ~25-fold faster than the value obtained for k_{cat} ($2.3 \pm 0.2\ s^{-1}$) in steady-state kinetic studies (Table 1). The results indicate that oxidation of P2C to DHP is not rate-limiting during turnover. The apparent second-order rate constant for the reaction of nikD with P2C, as estimated from stopped-flow data ($k_{lim}/K_{d\ app} = 2.0 \pm 0.2 \times 10^5\ M^{-1}\ s^{-1}$), is in excellent agreement with a value calculated using steady-state kinetic parameters ($k_{cat}/K_{m\ P2C} = 2.0 \pm 0.3 \times 10^5\ M^{-1}\ s^{-1}$) (Table 1). About 7% of the total absorbance decrease at 456 nm occurs in a second slow phase. The observed rate of the slow phase ($k_{slow} = 2.7 \pm 0.1$) is independent of the concentration of P2C (Figure 5B) and virtually identical to the value obtained for k_{cat} (Table 1). The results show that the slow phase is kinetically competent and probably rate-determining during turnover. The slow phase is attributed to an isomerization of the initial reduced enzyme·DHP complex (Scheme 3), as will be discussed.

Spectral Course of the Anaerobic Reduction of NikD with Unlabeled P2C. The spectral perturbations and kinetics observed for the formation of nikD·inhibitor complexes suggested that binding of P2C would also occur in a relatively slow reaction, accompanied by a substantial increase in absorbance in the 456 nm region. In this case, ES complex formation might overlap with the onset of enzyme reduction, a scenario that could account for the initial lags observed when enzyme reduction is monitored at 456 nm. Preliminary evidence consistent with this hypothesis was obtained by comparing the absorption spectrum of free nikD with spectra observed 0.74 ms after mixing the enzyme with various concentrations of P2C. The resulting difference spectra do indeed exhibit an increase in absorption in the 456 nm region, with positive bands at ~440 and ~465 nm (Figure 6). Furthermore, an excellent fit to the total absorbance change observed at 456 nm during nikD reduction is obtained by fitting a triple-exponential equation to the data, as illustrated by results obtained for the reaction with 100 μM P2C, which exhibits a prominent initial lag (see Figure 5A). The results are consistent with an initial, albeit undetected, time-dependent increase in absorbance at 456 nm due to ES complex formation. It is worth noting that difference spectra observed immediately after mixing nikD with P2C exhibit evidence of charge-transfer

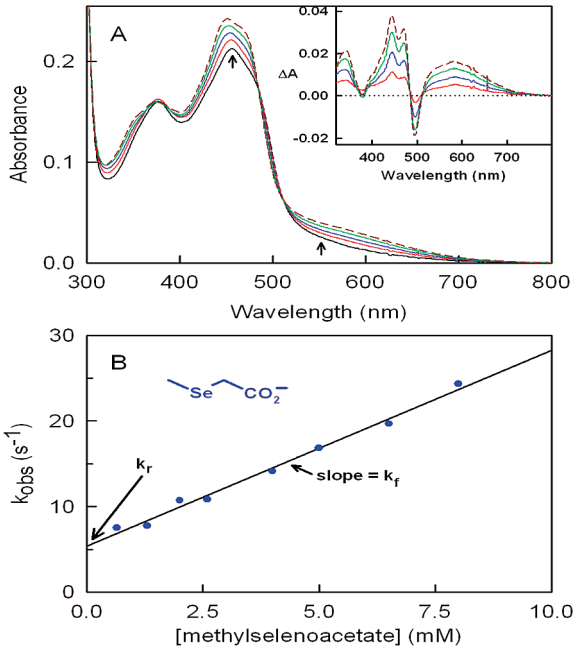

FIGURE 4: Spectral properties of the nikD·methylselenoacetate complex and the kinetics of complex formation. Binding of methylselenoacetate was monitored in 100 mM potassium phosphate buffer at pH 8.0 at 25 °C. Panel A shows a steady-state titration of nikD with methylselenoacetate. Arrows indicate the directions of the observed spectral changes. The black curve is the spectrum of free nikD. The solid red, blue, and green curves were recorded after the addition of 0.40, 1.19, and 4.33 mM methylselenoacetate, respectively. The dashed brown curve is the spectrum calculated for 100% complex formation, as described in Experimental Procedures. The inset shows the corresponding difference spectra, calculated by subtracting the spectrum observed for free nikD. Panel B shows the effect of methylselenoacetate concentration on the observed rate of complex formation, as monitored at 444 nm using a stopped-flow spectrometer in photomultiplier mode. The solid line was obtained by linear regression analysis of the data (blue circles).

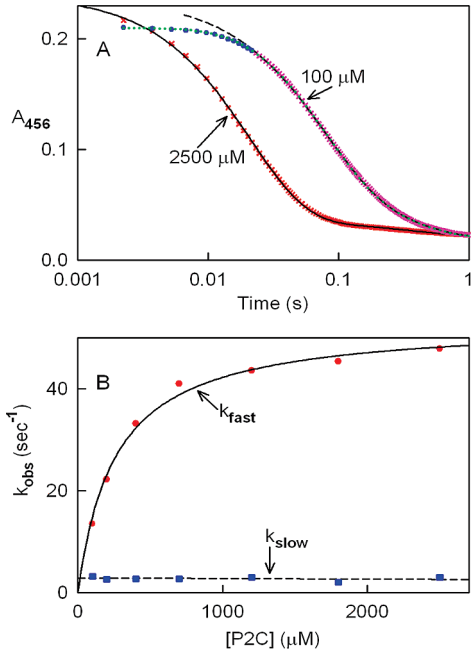

FIGURE 5: Kinetics of the anaerobic reduction of nikD with unlabeled P2C. The reaction was conducted in 100 mM potassium phosphate buffer at pH 8.0, at 25 °C and monitored using a stopped-flow spectrometer. Reaction traces at 456 nm were extracted from diode array data sets. Panel A: The solid black line was obtained by fitting a double-exponential equation ($y = Ae^{-k_{fast}t} + Be^{-k_{slow}t} + C$) to absorbance changes observed at 456 nm with 2500 μM P2C (red X's). The dashed black line was obtained by fitting a double-exponential equation to absorbance changes observed at 456 nm with 100 μM P2C (magenta X's), after excluding data points in the initial lag phase (blue circles). The dotted green line was obtained by fitting a triple-exponential equation ($y = Ae^{-k_{initial}t} + Be^{-k_{fast}t} + Ce^{-k_{slow}t} + D$) to the complete reaction course observed at 456 nm with 100 μM P2C. The double- and triple-exponential fits of the 100 μM P2C data yielded similar values for k_{fast} and k_{slow}. Panel B: The solid black line was obtained by fitting a hyperbola ($k_{obs} = k_{lim}[P2C]/(K_{d\ app} + [P2C])$ to values obtained for k_{fast} (red circles) at different concentrations of P2C. The dotted black line was obtained by linear regression analysis of values obtained for k_{slow} (blue squares) at different concentrations of P2C.

interaction, as judged by the substantial increase in long-wavelength absorption ($\lambda > 575$ nm) (see Figure 6). This feature strongly suggests that the ES complex contains the electron-rich enamine tautomer of P2C and not the electron deficient iminium zwitterion, a species unlikely to act as a charge-transfer donor.

A nearly isosbestic spectral course is obtained for the reaction of nikD with 100 μM P2C, exhibiting apparent concomitant loss of absorption in the 456 nm and long-wavelength regions (Figure 7A). However, closer inspection reveals a small transient increase in absorption at $\lambda > \sim$535 nm during enzyme reduction (Figure 7A, inset). The magnitude and complexity of the small absorbance changes in the long-wavelength region become progressively more apparent at higher substrate concentrations, as illustrated by results obtained for the reaction with 2500 μM P2C (Figure 7B).

Turnover and Kinetics of the Reductive-Half-Reaction with Deuterium-Labeled P2C. The kinetics of ES complex formation and enzyme reduction with unlabeled P2C appear to be poorly resolved, as judged by the results described above. We reasoned that it might be possible to improve the kinetic resolution and directly observe a time-dependent formation of the ES complex by using deuterium-labeled P2C in order to slow

Scheme 3: Proposed Mechanism for the Anaerobic Reduction of nikD by P2C[a]

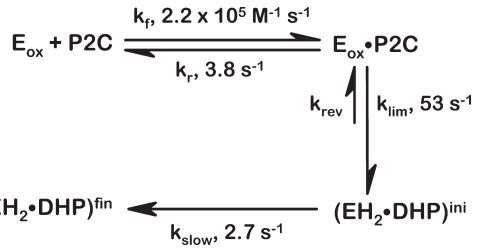

[a] E_{ox}·P2C is the ES charge-transfer complex; $(EH_2·DHP)^{ini}$ and $(EH_2·DHP)^{fin}$ are the reduced enzyme complexes formed in the fast and slow phases, respectively, of the reductive half-reaction, as discussed in the text. The oxidation of P2C to DHP is shown as a reversible reaction, as required based on the intersecting line double reciprocal plots obtained in steady-state kinetics studies. However, the observed hyperbolic dependence of k_{obs} on the concentration of P2C ($k_{obs} = k_{lim}[P2C]/(K_{d\ app} + [P2C])$ indicates that k_{rev} has a negligible value. Furthermore, values for k_{rev} that are not significantly different from zero are obtained upon fitting a 3-parameter hyperbolic equation ($k_{obs} = k_{rev} + k_{lim}[P2C]/(K_{d\ app} + [P2C])$ to the data.

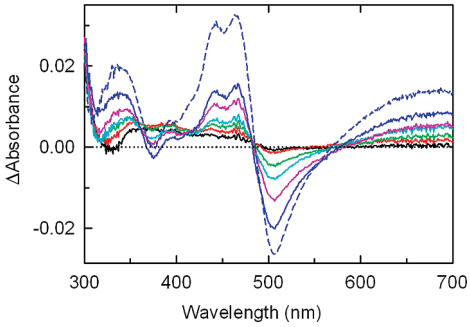

FIGURE 6: Calculated difference spectra for ES complex formation with nikD and P2C. Reactions with unlabeled or D_6-P2C were conducted with 18.6 or 18.9 μM nikD, respectively, in 100 mM potassium phosphate buffer at pH 8.0, at 25 °C and monitored using a stopped-flow diode array spectrometer. Difference spectra were obtained by subtracting the absorption spectrum of free nikD from spectra recorded 0.74 or 2.24 ms after mixing with unlabeled P2C or D_6-P2C, respectively, and have been normalized to the same enzyme concentration (18.6 μM). The solid black, red, green, cyan, magenta, and blue curves were calculated using data obtained with 100, 200, 400, 700, 1200, and 2500 μM unlabeled P2C, respectively. The dashed blue curve was obtained with 2500 μM D_6-P2C.

the rate of substrate oxidation. As detailed in Experimental Procedures, we used [3,3,4,4,5,5,6,6-D_8]-L-lysine as the starting compound in a multistep synthesis of deuterium-labeled P2C. The final step is conducted under acidic conditions and yields the hydrobromide salt of the imine tautomer, [3,3,4,4,5,5,6,6-D_8]-P2C (D_8-P2C). Solvent exchange at position C(3) in D_8-P2C will, however, occur at pH 8.0, owing to a facile interconversion between imine and enamine forms (*3*−*5*). Consequently, the deuterium-labeled substrate present in the pH 8.0 buffers used for kinetic studies is likely to contain 6 C-D bonds, [4, 4, 5, 5, 6, 6-D_6]-P2C, and will be referred to as D_6-P2C.

Double reciprocal plots that exhibit intersecting lines are obtained in steady-state kinetic studies with D_6-P2C (data not shown), consistent with a sequential mechanism, as observed with unlabeled P2C. The steady-state kinetic parameters determined with the deuterium-labeled substrate are listed in Table 1. Deuterium substitution causes a nearly 3-fold decrease in turnover rate but does not significantly affect the apparent rate of reaction of the reduced enzyme with oxygen, as judged by values obtained for k_{cat} and $k_{cat}/K_{m\ oxygen}$, respectively, with unlabeled and D_6-P2C.

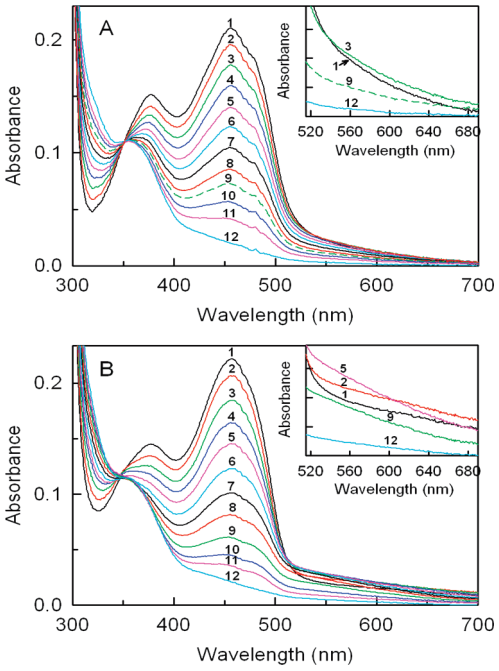

FIGURE 7: Spectral course of the anaerobic reduction of nikD with 100 μM (panel A) or 2500 μM (panel B) unlabeled P2C. Reactions were conducted in 100 mM potassium phosphate buffer at pH 8.0, at 25 °C and monitored using a stopped-flow diode array spectrometer. Spectra were recorded from 0.74 ms (curve 1) to 7.13 s (curve 12) after mixing. For selected spectra, an expanded view of the 515 to 690 nm region is shown in the insets. In panel A, curves 2 to 11 were recorded at 17.2, 29.2, 41.2, 55.5, 70.5, 91.5, 122, 150, 204, and 300 ms, respectively, after mixing. In panel B, curves 2 to 11 were recorded at 3.74, 6.74, 9.74, 12.7, 17.2, 23.2, 30.7, 42.7, 61.5, 91.5 ms, respectively, after mixing.

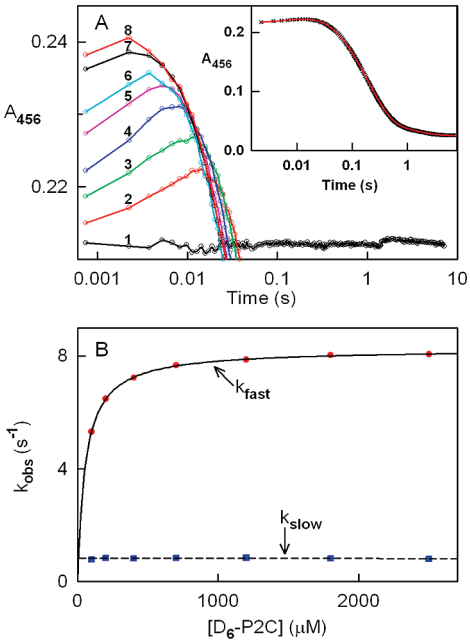

FIGURE 8: Kinetics of the anaerobic reduction of nikD with deuterium-labeled P2C. Reactions were conducted in 100 mM potassium phosphate buffer at pH 8.0, at 25 °C and monitored using a stopped-flow spectrometer. Reaction traces at 456 nm were extracted from diode array data sets. Panel A shows an expanded view of the initial phase of the reaction where an increase in absorbance at 456 nm is observed. Curves 1 to 8 were recorded after mixing nikD with 0, 100, 200, 400, 700, 1200, 1800, or 2500 μM D_6-P2C, respectively. The inset shows the complete trace for the reaction observed at 456 nm with 100 μM D_6-P2C. The solid red line was obtained by fitting a triple-exponential equation ($y = Ae^{-k_{initial}t} + Be^{-k_{fast}t} + Ce^{-k_{slow}t} + D$) to the entire data set (black X's). Similar values for k_{fast} and k_{slow} were obtained by fitting a double-exponential equation ($y = Ae^{-k_{fast}t} + Be^{-k_{slow}t} + C$) to only the observed decrease in absorbance at 456 nm (fit not shown, see Table 1). Panel B: The solid black line was obtained by fitting a hyperbola ($k_{obs} = k_{lim}[P2C]/(K_{d\ app} + [P2C])$ to values obtained for k_{fast} (red circles) at different concentrations of P2C. The dotted black line was obtained by linear regression analysis of values obtained for k_{slow} (blue squares) at different concentrations of P2C.

The effect of deuterium substitution on the kinetics of P2C oxidation to DHP was determined in reductive half-reaction studies. Importantly, an initial lag is not observed when the anaerobic reaction of nikD with D_6-P2C is monitored at 456 nm. Instead, an initial time-dependent increase in absorbance is observed and attributed to ES complex formation (Figure 8A). This initial phase is followed by a biphasic decrease in absorbance at 456 nm, similar to that seen with unlabeled P2C. An excellent fit is obtained by fitting a triple-exponential equation ($y = Ae^{-k_{initial}t} + Be^{-k_{fast}t} + Ce^{-k_{slow}t} + D$) to the total absorbance change observed at 456 nm, as illustrated by results obtained for the reaction with 100 μM D_6-P2C (Figure 8A, inset)[2]. About 94% of the total observed absorbance decrease at 456 nm occurs in a fast phase. The observed rate of this phase (k_{fast}) exhibits a hyperbolic dependence on the concentration of P2C ($k_{obs} = k_{lim}[P2C]/(K_{d\ app} + [P2C])$ (Figure 8B). The observed rate of the slow phase (k_{slow}) is independent of the concentration of P2C (Figure 8B)[3]. The latter two features are similar to that observed with unlabeled P2C (see Figure 5).

The limiting rate of nikD reduction at saturating D_6-P2C ($k_{lim} = 8.25 \pm 0.01\ s^{-1}$) is more than 6-fold slower than that observed with unlabeled P2C (KIE = 6.4 ± 0.1)[4] but nearly an order of magnitude faster than the turnover rate observed with D_6-P2C ($k_{cat} = 0.89 \pm 0.04\ s^{-1}$) (Table 1). The results indicate that oxidation of deuterium-labeled P2C to DHP is not rate-limiting during turnover. The apparent second-order rate constant for the reaction of nikD with D_6-P2C, as estimated from reductive half-reaction studies ($k_{lim}/K_{d\ app} = 1.49 \pm 0.02 \times 10^5\ M^{-1}\ s^{-1}$), is in moderately good agreement with a value calculated using steady-state kinetic parameters ($k_{cat}/K_{m\ P2C} = 0.74 \pm 0.07 \times 10^5\ M^{-1}\ s^{-1}$). The rate observed for the slow phase of the reductive half-reaction with D_6-P2C ($k_{slow} = 0.822 \pm 0.008\ s^{-1}$) is more than 3-fold slower than observed with unlabeled P2C (KIE = 3.3 ± 0.1)[4] but essentially identical to the value obtained for k_{cat} with D_6-P2C. The observed isotope effect indicates that the slow phase cannot simply reflect product release or a protein conformational change but must involve cleavage of one or more C−H bonds in the DHP intermediate, as will be discussed. The results also show that the slow phase observed with D_6-P2C is kinetically competent and likely to be rate-determining during turnover with D_6-P2C. This outcome agrees with results obtained with unlabeled P2C and indicates that deuterium substitution has not changed the apparent rate-determining step during turnover.

Spectral Course of the Anaerobic Reduction of NikD with Deuterium-Labeled P2C. Maximal formation of the ES complex with 400 μM D_6-P2C is observed 10 ms after mixing, as

[2]The data do not permit accurate determination of values for $k_{initial}$ because of the small spectral change and the limited number of points contained within the initial phase in 456 nm absorbance traces extracted from diode-array data sets.

[3]Similar values for k_{fast} and k_{slow} were obtained by biphasic analysis of the absorbance decrease at 456 nm (see Table 1).

[4]The observed value is likely to include both primary and secondary KIEs.

judged by the observed increase in absorbance at 456 nm (see Figure 8A). Spectra recorded during the initial 10 ms of this reaction show that ES complex formation results in isosbestic absorption increases in the 456 nm and long-wavelength regions (Figure 9A, inset). The rest of the reaction (t > 10 ms) proceeds with a concomitant loss of absorption in both regions, exhibiting a nearly isosbestic spectral course (Figure 9A, main panel). The data provide no evidence for a small transient increase in long-wavelength absorption during enzyme reduction, unlike results obtained with a low concentration of unlabeled P2C (see Figure 7A, inset).

The rate observed for the fast phase of enzyme reduction with 400 μM D_6-P2C is close to the limiting rate of this step (see Figure 8B). Higher concentrations of D_6-P2C mainly serve to increase the rate of ES complex formation. Consequently, the time required for maximal ES complex formation is shortened, the apparent maximal yield of the intermediate is increased and a greater proportion of the reaction occurs during mixing at higher substrate concentrations, as can be seen by inspection of the initial absorbance traces at 456 nm (see Figure 8A). These traces indicate that the maximal yield of the ES complex observed in these studies is attained 2.24 ms after mixing with 2500 μM D_6-P2C, the highest substrate concentration tested. The spectral perturbation due to ES complex formation with 2500 μM D_6-P2C was estimated by subtracting the absorption spectrum of free nikD from that observed at 2.24 ms after mixing. The calculated difference spectrum is qualitatively similar, but much greater in magnitude, compared with that seen for the same reaction with unlabeled P2C (see Figure 6). This difference is attributed to the enhanced kinetic resolution of binding and oxidation steps that is achieved with the deuterium-labeled substrate.

The spectral course observed for conversion of the ES complex, formed with 2500 μM D_6-P2C, to the final reduced enzyme species (Figure 9B) is similar to that observed for the corresponding reaction with 400 μM D_6-P2C (Figure 9A), except for a small transient increase in long-wavelength absorption that is observed during reduction at the higher substrate concentration (Figure 9B, inset). The small transient increase in long-wavelength absorption is, however, much less pronounced compared with that observed for the reaction with the same concentration of unlabeled P2C (see Figure 7B, inset). The reason for this difference is unclear.

Calculated Spectral Properties of Postulated Reaction Intermediates. Global analysis was performed by fitting a model, A → B → C → D, to spectra acquired in reductive half-reaction studies with D_6-P2C. In this model, species A is free nikD, intermediate B is the putative oxidized enzyme·P2C charge-transfer complex, intermediate C is the postulated reduced enzyme·DHP complex formed in the fast phase of enzyme reduction, and D is the reduced enzyme species observed at the end of the reductive half-reaction (see Scheme 3). A good fit of the proposed model was obtained. Kinetic parameters for the reductive half-reaction obtained by global analysis are in very good agreement with values obtained by analysis of absorbance changes at 456 nm (see Table 1). Similar absorption spectra are calculated for the intermediates by analysis of reactions at different substrate concentrations.

The calculated absorption spectrum of intermediate B exhibits increased absorption in the long-wavelength region, as expected for a charge-transfer complex, and is very similar to the spectrum observed 2.24 ms after mixing nikD with 2500 μM D_6-P2C

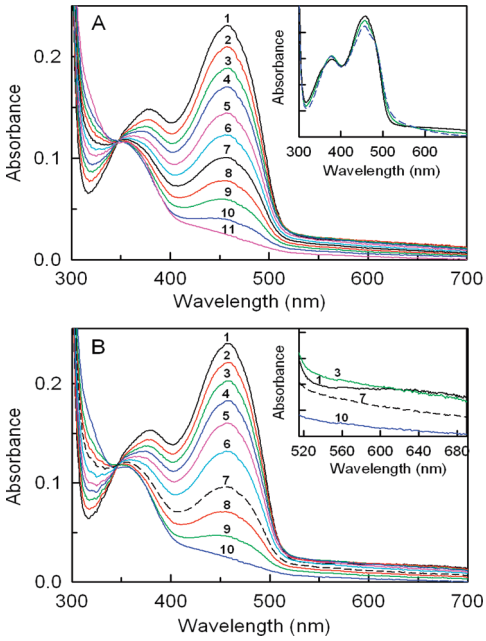

FIGURE 9: Spectral course of the anaerobic reduction of nikD with 400 μM (panel A) or 2500 μM (panel B) deuterium-labeled P2C. Reactions were conducted in 100 mM potassium phosphate buffer at pH 8.0, at 25 °C and monitored using a stopped-flow diode array spectrometer. Panel A: The inset shows the initial phase of the reaction (ES complex formation) observed with 400 μM D_6-P2C. The dashed blue line is the spectrum of free nikD. The green and black curves were recorded 0.74 and 9.74 ms, respectively, after mixing. The main portion of the figure shows the spectral course of the reaction from 9.74 ms (curve 1) to 7.13 s (curve 11). Curves 2 to 10 were recorded 30.7, 49.5, 67.5, 97.5, 127.5, 168.0, 228.0, 306.0, and 507.0 ms, respectively, after mixing the enzyme with 400 μM D_6-P2C. Panel B: The main portion of the figure shows the spectral course of the reaction from 2.24 ms (curve 1, ES complex) to 7.13 s (curve 10). Curves 2 to 9 were recorded 17.2, 32,2, 49.5, 70.5, 103.5, 162.0, 228.0, and 363.0 ms, respectively, after mixing the enzyme with 2500 μM D_6-P2C. For selected spectra, the inset shows an expanded view of the long-wavelength region, comparable to that shown for the corresponding reaction with 2500 μM unlabeled P2C (see Figure 7B).

(Figure 10). The calculated absorption spectrum of intermediate C is consistent with that expected for a reduced flavoenzyme but exhibits modest differences, including higher absorbance in the 456 nm region, compared with the observed spectrum of the final reduced enzyme species (D). The calculated intermediate absorption spectra were used to estimate the fraction of the total absorbance decrease at 456 nm that would occur in the fast phase under conditions that promote quantitative ES complex formation [$f = (\varepsilon_B - \varepsilon_C)/(\varepsilon_B - \varepsilon_D)$] versus conditions where negligible accumulation occurs because of poor kinetic resolution of binding and oxidation steps [$f = (\varepsilon_A - \varepsilon_C)/(\varepsilon_A - \varepsilon_D)$]. The calculated fractions for the two extremes are quite similar (0.957 and 0.949, respectively) and in good agreement with values obtained upon kinetic analysis of the biphasic absorbance decrease observed at 456 nm in reductive half-reactions with D_6-P2C (0.944 ± 0.004) or unlabeled substrate (0.935 ± 0.004).

Calculated Rates for Formation and Dissociation of the Enzyme·Substrate Charge-Transfer Complex. As described above, the rate observed for the conversion of the ES complex to the initial reduced enzyme·DHP complex exhibits a hyperbolic dependence on the concentration of P2C ($k_{obs} = k_{lim}$[P2C]/($K_{d\ app}$ + [P2C]). The value obtained for $K_{d\ app}$ with D_6-P2C is nearly 5-fold smaller than observed with unlabeled substrate (Table 1). For the mechanism shown in Scheme 3, $K_{d\ app}$ is equal

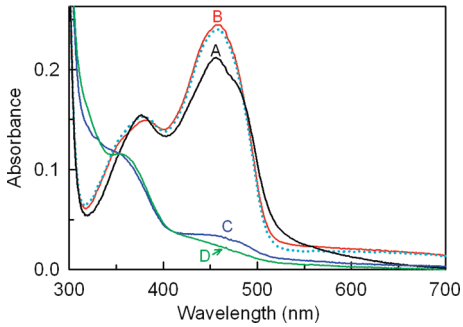

FIGURE 10: Calculated absorption spectra for intermediates formed during the anaerobic reduction of nikD with P2C. Spectra were calculated by global fitting of a model, A → B → C → D, to diode-array stopped-flow data obtained for the reaction with D_6-P2C, as detailed in the text. The black curve (A) is the spectrum of free nikD (18.9 μM). The green curve (D) is the final observed spectrum of the reduced enzyme species formed in the reductive half-reaction. The red curve (B) is the calculated spectrum of the oxidized enzyme·P2C charge transfer complex. The blue curve (C) is the calculated spectrum of the reduced enzyme species formed in the fast phase of enzyme reduction. The dotted cyan curve is the spectrum observed 2.24 ms after mixing nikD with 2500 μM D_6-P2C.

to the ratio $(k_r + k_{lim})/k_f$. Deuterium substitution is unlikely to affect the rate of ES complex formation (k_f) or dissociation (k_r). An isotope effect on $K_{d\ app}$ is expected for a sticky substrate ($k_r \ll k_{lim}$) but not for a nonsticky substrate ($k_r \gg k_{lim}$) where the value obtained for $K_{d\ app}$ is equal to the true dissociation constant for the ES complex ($K_d = k_r/k_f$). The results strongly suggest that P2C is a sticky substrate for nikD. Values for k_f, k_r, and K_d for the ES complex were calculated using values obtained for k_{lim} and $K_{d\ app}$ with unlabeled and deuterium-labeled P2C. The calculated parameters for the nikD·P2C complex are very similar to k_f, k_r, and K_d values obtained for the nikD complex formed with CHA, a competitive inhibitor, and 1-deaza analogue of the enamine form of P2C (Table 2).

The calculated value for the rate of dissociation of the nikD·P2C complex ($k_r = 3.8 \pm 0.3\ s^{-1}$) is more than an order of magnitude slower than the limiting rate obtained for oxidation of unlabeled P2C to DHP ($k_{lim} = 53 \pm 1\ s^{-1}$), as expected for a sticky substrate. For the mechanism shown in Scheme 3, the ratio $k_{lim}/K_{d\ app}$ (or $k_{cat}/K_{m\ P2C}$) is equal to a collection of rate constants, $k_{lim}k_f/(k_r + k_{lim})$. However, for a sticky substrate ($k_r \ll k_{lim}$) the ratio will be equal to k_f, the second-order rate constant for ES complex formation. Consistent with this prediction, the value observed for $k_{lim}/K_{d\ app}$ (or $k_{cat}/K_{m\ P2C}$) with unlabeled P2C ($2.0 \pm 0.2 \times 10^5\ M^{-1}s^{-1}$) is, within experimental error, identical to the estimated value for k_f ($2.2 \pm 0.2 \times 10^5\ M^{-1}\ s^{-1}$). The value observed for $k_{lim}/K_{d\ app}$ with D_6-P2C is about 30% smaller than the estimated value for k_f. This outcome is consistent with the fact that the estimated rate of ES complex dissociation is only 2-fold slower than the limiting rate obtained for the 2-electron oxidation of D_6-P2C ($k_{lim} = 8.25 \pm 0.01\ s^{-1}$).

DISCUSSION

Substrate analogues bind to nikD in a relatively slow reaction and induce substantial changes in the visible absorption spectrum of the enzyme that can be readily monitored at 25 °C by using a stopped-flow spectrometer. Similar kinetics are observed for complex formation with several competitive inhibitors, including electron-poor (CHA) and electron-rich (MeSeA) analogues of the enamine form of P2C, and picolinate, the product of the 4-electron oxidation of P2C. In each case, apparent first-order rate constants observed for complex formation exhibit a linear dependence on ligand concentration with a finite *y*-intercept, consistent with a simple one-step approach to equilibrium. The results provide no evidence for a two-step binding mechanism, previously proposed based on structures observed for open and closed forms of the nikD·picolinate complex (*20*). Trp355 is apparently stacked above the flavin ring in the major form present in solutions of ligand-free nikD at pH 8.0, as judged by the observed charge transfer band. In the two-step model, ligands were thought to form an initial complex where the indole ring of Trp355 remained parallel to the flavin ring, followed by displacement of Trp355 in a spectrally detectable step to produce a more stable complex with ligand stacked above the flavin ring. To account for the observed binding kinetics, we postulate that ligands bind to a minor form where Trp355 is perpendicular to the flavin to produce a complex with ligand stacked above the flavin in a single, spectrally detectable step. The second-order rate constant determined for complex formation (k_f) with competitve inhibitors is positively correlated with complex stability: CHA > picolinate > MeSeA. However, even the most tightly bound inhibitor (CHA, $K_d = 12.8\ \mu M$) binds at a rate ($k_f = 1.08 \times 10^5\ M^{-1}\ s^{-1}$) that is orders of magnitude slower than predicted for a diffusion-limited reaction (10^8–$10^{10}\ M^{-1}\ s^{-1}$). As pointed out by Knowles (*27*), values below this range may be obtained if the ligand binds to a minor enzyme form, as proposed for nikD.

The initial phase observed during the anaerobic reaction of nikD with P2C is attributed to a relatively slow formation of an ES complex that exhibits higher absorbance at 456 nm and also in the long-wavelength region ($\lambda > 575$ nm), a diagnostic feature of charge-transfer interaction. The complex is likely to contain the electron-rich enamine tautomer of P2C because the electron-deficient iminium zwitterion is unlikely to act as a charge-transfer donor. Significantly, a charge transfer complex is also observed with MeSeA but not detected with electron-poor substrate analogues. The observed ES charge-transfer complex is consistent with the proposal that the initial oxidation of P2C occurs at the bond between N(1) and C(6) (see Scheme 1), a reaction possible only with the enamine tautomer. Substrate binding and oxidation steps are poorly resolved when the reductive half-reaction is conducted with unlabeled P2C. Under these conditions, ES complex formation is detectable as an initial lag when the reaction is monitored at 456 nm and by the spectral perturbation observed immediately ($t = 0.74$ ms) after mixing. A time-dependent formation of the ES complex is, however, directly observed with D_6-P2C because of a slower rate of substrate oxidation.

The second phase of the reductive half-reaction is associated with conversion of the ES complex to a reduced enzyme·DHP complex, $(EH_2 \cdot DHP)^{ini}$ (see Scheme 3). The observed rate of this step exhibits a hyperbolic dependence on substrate concentration ($k_{obs} = k_{lim}[P2C]/(K_{d\ app} + [P2C])$. The limiting rate obtained for nikD reduction at saturating P2C is at least 10-fold faster than the turnover rate observed with labeled or unlabeled substrate and exhibits a substantial kinetic isotope effect (KIE = 6.4 ± 0.1)[4]. P2C is a sticky substrate, as judged by the observed kinetic isotope effect on $K_{d\ app}$ (KIE = 4.7 ± 0.4)[4]. Values for the rate of formation ($k_f = 2.2 \times 10^5\ M^{-1}\ s^{-1}$), dissociation ($k_r = 3.8\ s^{-1}$), and stability ($K_d = 17\ \mu M$) of the nikD·P2C complex were estimated on the basis of the observed isotope effects on k_{cat} and $K_{d\ app}$. The calculated parameters are very similar to those observed for the corresponding complex with CHA, a 1-deaza

analogue of the enamine tautomer (see Table 2). The estimated micromolar binding affinity of nikD for P2C, combined with the fact that P2C acts as a sticky substrate, may represent an evolutionary adaptation designed to prevent cellular accumulation of P2C, a compound that is fairly unstable under physiological conditions.

The calculated absorption spectrum of the initial reduced enzyme·DHP complex, $(EH_2 \cdot DHP)^{ini}$, is typical of that expected for a reduced flavoenzyme but exhibits somewhat higher absorbance in the 456 nm region and other differences compared with a final reduced species, $(EH_2 \cdot DHP)^{fin}$, that is formed in the third phase of the reductive half-reaction. The observed rate of the final step is independent of the substrate concentration, virtually identical to the turnover rate observed with labeled or unlabeled P2C, and exhibits a significant kinetic isotope effect (KIE = 3.3 ± 0.1)[4]. The results indicate that the last phase is kinetically competent and probably rate-determining during turnover. The observed isotope effect indicates that this step cannot involve a simple conformational change and/or product release. The results are consistent with a sequential mechanism where oxygen reacts with a reduced enzyme·DHP complex to yield an oxidized enzyme·DHP complex, as proposed on the basis of results obtained in steady-state kinetic studies. Additional evidence that argues against dissociation of any reduced enzyme·DHP complex during turnover is provided by oxidative half-reaction studies, which show that free reduced nikD is not a kinetically competent intermediate[5]. Appreciable dissociation of the oxidized enzyme·DHP complex is also unlikely because DHP oxidation to picolinate is probably at least an order of magnitude faster than DHP release, as judged by values obtained for the corresponding reactions with P2C. Consistent with this hypothesis, the steady-state data provide no evidence for excess substrate inhibition, a feature that would be expected if DHP were released because substrate and the labile intermediate would then compete in binding to the oxidized enzyme.

The kinetic isotope effect observed for the last step of the reductive half-reaction indicates that conversion of $(EH_2 \cdot DHP)^{ini}$ to $(EH_2 \cdot DHP)^{fin}$ must involve cleavage of one or more C−H bond in the DHP intermediate. A protonated DHP imine is produced during the proposed initial 2-electron oxidation of the P2C enamine (Scheme 4, step 1). Ionization of the protonated DHP imine will yield the corresponding neutral DHP enamine (Scheme 4, step 2), as judged by the analogous tautomerization reaction observed with free P2C (pK_a = 8.2) (*4*, *5*). Isomerization of the initially formed DHP enamine (A) will generate a more stable isomer with conjugated double bonds (B) (Scheme 4, step 3). We propose that nikD oxidizes the bond between N(1) and C(6) in isomer B to yield picolinate (Scheme 4, step 4). The proposed mechanism allows nikD to catalyze a remarkable aromatization reaction by effectively oxidizing the same bond twice, a scenario that circumvents the need to reposition FAD and/or the DHP intermediate. Such movements would be required to allow oxidation of different bonds while satisfying the geometric constraints observed for flavoenyzme-catalyzed reactions (*15*, *28*). However, the flavin in nikD is covalently tethered to the protein and not likely to assume different positions during turnover, in contrast to the mobile flavin in *p*-hydroxybenzoate hydroxylase (*29*). Furthermore, motion of the DHP intermediate is probably highly constrained by an aromatic cage surrounding the DHP ring plus hydrogen bonding to the DHP carboxylate, as judged by the structure observed for the closed nikD·picolinate complex (*15*). These restrictions might be relaxed by conversion to an open complex (*15*), but this change in protein conformation is likely to promote a counterproductive release of the DHP intermediate. A catalytic strategy, similar to that proposed in Scheme 4 for nikD, may be utilized by other flavoenzymes that catalyze the aromatization of L-proline residues to yield pyrrole-2-carboxyl units that are essential components of various nonribosomally synthesized peptidyl antibiotics (e.g., chlorobiocin and pyoluteorin) (*30*, *31*).

Scheme 4: Possible Mechanism for the Conversion of P2C to Picolinate Involving Tautomerization and Isomerization of a DHP Intermediate Bound to Reduced nikD[a]

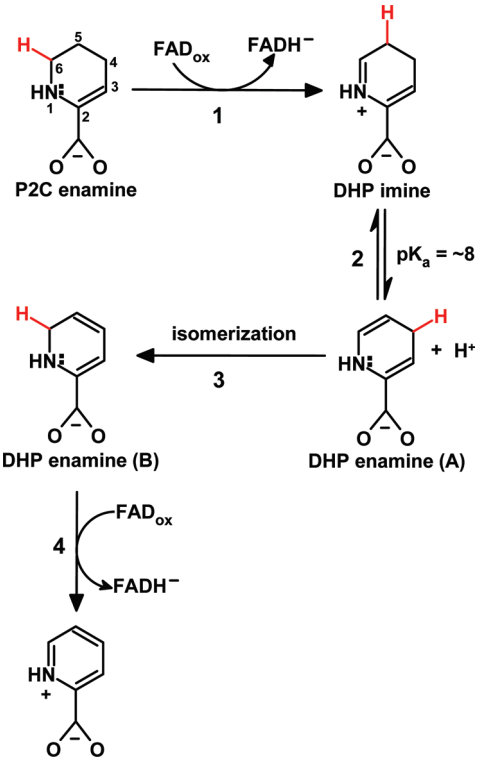

[a] The CH bond that is cleaved in each step is shown in red.

ACKNOWLEDGMENT

We are grateful to Dr. Louis Silks (National Stable Isotope Resource at Los Alamos) for his generous gift of methylselenoacetate. We thank Dr. Phaneeswara-Rao Kommoju for valuable technical assistance.

REFERENCES

1. Hector, R. F. (1993) Compounds active against cell walls of medically important fungi. *Clin. Microb. Rev. 6*, 1–21.
2. Bruntner, C., and Bormann, C. (1998) The *Streptomyces tendae Tu901* L-lysine 2-aminotransferase catalyzes the initial reaction in nikkomycin D biosynthesis. *Eur. J. Biochem. 254*, 347–355.
3. Macholan, L., and Svatek, E. (1960) Aminoketocarbonsauren VL: Über die konstitution and strukturformen der α-keto-analoga natürlichler diaminosäuren, *Collection Czechoslov. Chem. Commun. 25*, 2564–2575.
4. Srinivasan, R., and Fisher, H. F. (1986) Structural features facilitating the glutamate dehydrogenase catalyzed α-imino acid-α-amino acid interconversion. *Arch. Biochem. Biophys. 246*, 743–750.
5. Jorns, M. S., Bruckner, R. C., Zhao, G., Carrell, C. J., and Mathews, F. S. (2005) NikD: Crystal Structures, Charge Transfer Complex and Endogenous Ligands, in *Flavins and Flavoproteins* (Nishino, T.,

[5] Kommoju, P. R., Bruckner, R. C., and Jorns, M. S., unpublished results.

Miura, R., Tanokura, M., and Fukui, K., Eds.) pp 773−785, ARchi-Tech Inc., Tokyo, Japan.
6. Bruckner, R. C., Zhao, G., Venci, D., and Jorns, M. S. (2004) Nikkomycin biosynthesis: Formation of a 4-electron oxidation product during turnover of nikD with its physiological substrate. *Biochemistry 43*, 9160–9167.
7. Venci, D., Zhao, G., and Jorns, M. S. (2002) Molecular characterization of nikD, a new flavoenzyme important in the biosynthesis of nikkomycin antibiotics. *Biochemistry 41*, 15795–15802.
8. Khanna, P., and Jorns, M. S. (2001) Characterization of the FAD-containing N-methyltryptophan oxidase from *Escherichia coli*. *Biochemistry 40*, 1441–1450.
9. Wu, X. L., Takahashi, M., Chen, S. G., and Monnier, V. M. (2000) Cloning of amadoriase I isoenzyme from *Aspergillus sp.*: Evidence of FAD covalently linked to Cys342. *Biochemistry 39*, 1515–1521.
10. Miura, S., Ferri, S., Tsugawa, W., Kiin, S., and Sode, K. (2006) Active site analysis of fructosyl amine oxidase using homology modeling and site-directed mutagenesis. *Biotechnol. Lett. 28*, 1895–1900.
11. Dodt, G., Kim, D. G., Reimann, S. A., Reuber, B. E., McCabe, K., Gould, S. J., and Mihalik, S. J. (2000) L-pipecolic acid oxidase, a human enzyme essential for the degradation of L-pipecolic acid, is most similar to the monomeric sarcosine oxidases. *Biochem. J. 345*, 487–494.
12. Wagner, M. A., Khanna, P., and Jorns, M. S. (1999) Structure of the flavocoenzyme of two homologous amine oxidases: Monomeric sarcosine oxidase and N-methyltryptophan oxidase. *Biochemistry 38*, 5588–5595.
13. Trickey, P., Wagner, M. A., Jorns, M. S., and Mathews, F. S. (1999) Monomeric sarcosine oxidase: Structure of a covalently-flavinylated secondary amine oxidizing enzyme. *Structure 7*, 331–345.
14. Barriere, J. C., Berthaud, N., Beyer, D., Dutka-Malen, S., Paris, J. M., and Desnottes, J. F. (1998) Recent developments in streptogramin research. *Curr. Pharm. Des. 4*, 155–180.
15. Carrell, C. J., Bruckner, R. C., Venci, D., Zhao, G., Jorns, M. S., and Mathews, F. S. (2007) NikD, an unusual amino acid oxidase essential for nikkomycin biosynthesis: Structures of closed and open forms at 1.15 and 1.90 Å resolution. *Structure 15*, 928–941.
16. Ghanem, M., Fan, F., Francis, K., and Gadda, G. (2003) Spectroscopic and kinetic properties of recombinant choline oxidase from *Arthrobacter globiformis*. *Biochemistry 42*, 15179–15188.
17. Gomez-Moreno, C., and Edmondson, D. E. (1985) Evidence for an aldehyde intermediate in the catalytic mechanism of thiamine oxidase. *Arch. Biochem. Biophys. 239*, 46–52.
18. Schuman, M., and Massey, V. (1972) Purification and characterization of glycolic acid oxidase from pig liver. *Biochim. Biophys. Acta 227*, 500–520.
19. Ghosh, D., Griswold, J., Erman, M., and Pankhurst, K. L. (2009) Structural basis for androgen specificity and oestrogen synthesis in human aromatase. *Nature (London) 457*, 219–223.
20. Bruckner, R. C., Zhao, G., Ferreira, P., and Jorns, M. S. (2007) A mobile tryptophan is the intrinsic charge transfer donor in a flavoenzyme essential for nikkomycin antibiotic biosynthesis. *Biochemistry 46*, 819–827.
21. Hafner, E. W., and Wellner, D. (1971) Demonstration of imino acids as products of the reactions catalyzed by D- and L-amino acids oxidases. *Proc. Natl. Acad. Sci. U.S.A. 68*, 987–991.
22. Raibekas, A. A., and Massey, V. (1997) Glycerol-assisted restorative adjustment of flavoenzyme conformation perturbed by site-directed mutagenesis. *J. Biol. Chem. 272*, 22248–22252.
23. Wagner, M. A., and Jorns, M. S. (2000) Monomeric sarcosine oxidase: 2. Kinetic studies with sarcosine, alternate substrates and substrate analogues. *Biochemistry 39*, 8825–8829.
24. Neuberger, A., and Sanger, F. (1943) The availability of the acetyl derivatives of lysine for growth. *Biochem. J. 37*, 515–518.
25. Nowshuddin, S., and Reddy, A. R. (2006) Decomposition of copper-amino acid complexes by sodium sulfide. *Tetrahedron Lett. 47*, 5159–5161.
26. Zhao, G., and Jorns, M. S. (2006) Spectral and kinetic characterization of the Michaelis charge transfer complex in monomeric sarcosine oxidase. *Biochemistry 45*, 5985–5992.
27. Blacklow, S. C., Raines, R. T., Lim, W. A., Zamore, P. D., and Knowles, J. R. (1988) Triosephosphate isomerase catalysis is diffusion controlled. *Biochemistry 27*, 1158–1167.
28. Fraaije, M. W., and Mattevi, A. (2000) Flavoenzymes: diverse catalysts with recurrent features. *Trends Biol. Sci. 25*, 126–132.
29. Gatti, D. L., Palfey, B. A., Lah, M. S., Entsch, B., Massey, V., Ballou, D. P., and Ludwig, M. L. (1994) The mobile flavin of 4-OH benzoate hydroxylase. *Science 266*, 110–114.
30. Thomas, M. G., Burkart, M. D., and Walsh, C. T. (2002) Conversion of L-proline to pyrrolyl-2-carboxyl-S-PCP during undecylprodigiosin and pyoluteorin biosynthesis. *Chem. Biol. 9*, 171–184.
31. Garneau, S., Dorrestein, P. C., Kelleher, N. L., and Walsh, C. T. (2005) Characterization of the formation of the pyrrole moiety during clorobiocin and coumermycin A biosynthesis. *Biochemistry 44*, 2770–2780.